

# Supplemental Material for: When are Surface Plasmon Polaritons Excited in the Kretschmann-Raether configuration?

Jonathan J. Foley IV, Hayk Harutyunyan, Daniel Rosenmann, Ralu Divan, Gary P. Wiederrecht, Stephen K. Gray

March 9, 2015

## Contents

### List of Figures

S1	Schematic of 4 layer system. . . . .	3
S2	Schematic of conditions on wavevectors . . . . .	5
S3	FDTD simulation of K-R excitation of SPPs on glass/50 nm Au/air structure. . . . .	7
S4	Resonances in glass/50 nm gold/air structure . . . . .	8
S5	Comparison of PA and SPP Modes to Semi-Infinite SPP Dispersion . . . . .	9
S6	Comparison of reflectance and leakage with and without nanoparticles . . . . .	10
S7	Plot of s-wave PA mode in Sapphire/VO <sub>2</sub> /air structure . . . . .	11
S8	Plot of p-wave PA mode in Sapphire/VO <sub>2</sub> /air structure . . . . .	12

## General Development of Fresnel and Modal equations

### Fresnel Equations

Consider an L-layer system, with Figure 1 depicting the L = 4 case. The optical response in each layer  $j$  arises from the (in general) frequency-dependent refractive index,  $N_j(\omega) = n_j(\omega) + ik_j(\omega)$ , where  $n_j$  and  $k_j$  are real numbers. The associated electrical permittivity is  $\epsilon_j = N_j^2$ . Layers  $j = 1$  and  $j = L$  are semi-infinite, generally non-absorbing dielectric materials characterized by real, positive refractive indices,  $N_1 = n_1 > 0$  and  $N_L = n_L > 0$ . The central layers 2, ..., L-1 could include absorbing materials that are described by complex refractive indices. Metallic layers are absorbing but can also be such that  $\text{Re}(\epsilon_j) = \text{Re}(N_j^2) = n_j^2 - k_j^2 < 0$ . Since the films, with our coordinate system choice (Fig. 1), are homogeneous in the  $y$ -direction, the relevant tangential electrical field component is taken to be the real part of the phasor  $\exp(i(k_x x - \omega t)) E(z)$  with [1,2]

$$E(z) = \left\{ \begin{array}{ll} E_1^+ \exp(ik_{z1}z) + E_1^- \exp(-ik_{z1}z) & z < z_1 \equiv 0 \\ E_2^+ \exp(ik_{z2}(z - z_1)) + E_2^- \exp(-ik_{z2}(z - z_1)) & z_1 < z < z_2 \\ \dots & \dots \\ E_L^+ \exp(ik_{zL}(z - z_{L-1})) + E_L^- \exp(-ik_{zL}(z - z_{L-1})) & z > z_{L-1} \end{array} \right)$$

where the z-component of the wavevector in each layer satisfies

$$k_{zj} = \pm \sqrt{N_j^2 k_0^2 - k_x^2} \quad , \quad (1)$$

with  $k_0 = \omega/c$ . For  $p$ -polarized light  $E(z) \equiv E_x(z)$ , and for  $s$ -polarized light  $E(z) \equiv E_y(z)$ .

The boundary conditions for satisfying Maxwell's equations are that the tangential components of the magnetic (and electric) field be continuous across each interface, which leads to [1]:

$$\begin{pmatrix} E_1^+ \\ E_1^- \end{pmatrix} = D_1^{-1} D_2 \begin{pmatrix} E_2^+ \\ E_2^- \end{pmatrix}$$

and

$$\begin{pmatrix} E_l^+ \\ E_l^- \end{pmatrix} = P_l D_l^{-1} D_{l+1} \begin{pmatrix} E_{l+1}^+ \\ E_{l+1}^- \end{pmatrix}$$

for  $l = 1, \dots, L - 1$ . The matrix  $D_l$  is defined

$$D_l = \begin{pmatrix} \cos(\theta_l) & \cos(\theta_l) \\ N_l & -N_l \end{pmatrix}$$

for  $p$ -polarized light and

$$D_l = \begin{pmatrix} 1 & 1 \\ N_l \cos(\theta_l) & -N_l \cos(\theta_l) \end{pmatrix}$$

for  $s$ -polarized light. For the entire  $L$ -layer structure, we have

$$\begin{pmatrix} M_{11} & M_{12} \\ M_{21} & M_{22} \end{pmatrix} = D_1^{-1} \left( \prod_{l=2}^{L-1} D_l P_l D_l^{-1} \right) D_L,$$

where  $P_l$  is

$$P_l = \begin{pmatrix} \exp(-ik_{z_l} d_l) & 0 \\ 0 & \exp(ik_{z_l} d_l) \end{pmatrix}.$$

We are interested in the Fresnel solutions corresponding to Kretschmann-Raether (K-R) excitation and therefore imagine incident waves from the bottom,  $j = 1$ , semi-infinite layer, which we generally take to be an appropriate glass or prism material. Solving the matrix equation under consideration of such a specific incident wave is equivalent to solving the Fresnel equations for the  $L$ -layer structure, which can therefore be written as

$$\begin{pmatrix} E_1^+ = 1 \\ E_1^- = r \end{pmatrix} = \begin{pmatrix} M_{11} & M_{12} \\ M_{21} & M_{22} \end{pmatrix} \begin{pmatrix} E_L^+ = t \\ E_L^- = 0 \end{pmatrix}. \quad (2)$$

The reflection and transmission amplitudes are given by

$$r = \frac{M_{2,1}}{M_{1,1}} \quad (3)$$

and

$$t = \frac{1}{M_{1,1}}, \quad (4)$$

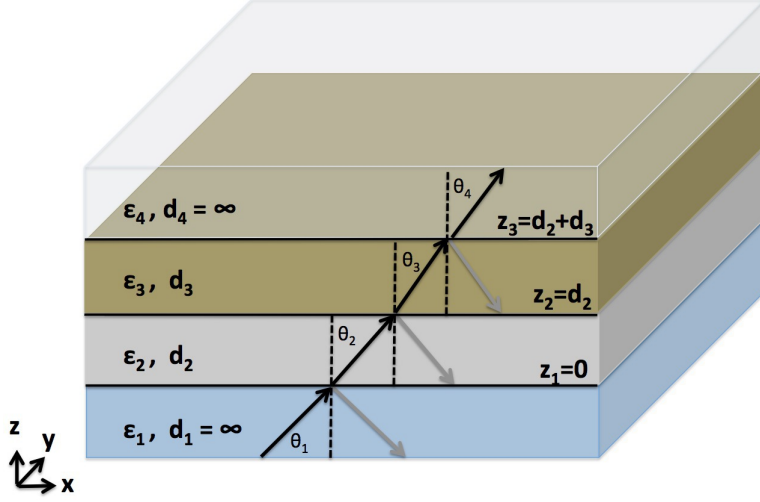


Figure S1: Schematic of 4 layer system with two absorbing layers with finite thickness ( $d_2$  and  $d_3$ ) sandwiched by 2 semi-infinite dielectric layers. Because we focus particular attention the modes accessible in K-R experiments, we assume  $\epsilon_1 > \epsilon_4$ .

and the reflection and transmission probabilities are

$$R = |r|^2 \quad (5)$$

and

$$T = \frac{n_L \cos(\theta_L)}{n_1 \cos(\theta_1)} |t|^2. \quad (6)$$

The  $x$  component of the wavevector is a positive real number,  $k_x = N_1 k_0 \sin(\theta_1)$ , with  $\theta_1$  being the real angle of incidence. The various  $k_{zj}$  for  $j = 2, \dots, L-1$  may be complex but the choices taken for the signs in Eq. 1 do not matter because each of these layers has both incoming and outgoing terms. Regarding  $k_{zL}$ , the physically acceptable solutions is either a real positive number or a purely imaginary value with positive imaginary part, the latter case corresponding to an evanescent wave in layer  $L$ . With all these specifications of  $k_x$  and the  $k_{zj}$ ,  $M_{1,1}$  and  $M_{2,1}$  and thus the transmission and reflection properties may be directly evaluated.

## Modal Equations

The modes supported by an arbitrary thin film structure must obey the same conditions on the tangential components of the fields as were imposed by Eq. (6). However, the modes are generally defined to satisfy

$$\begin{pmatrix} E_1^+ = 0 \\ E_1^- \end{pmatrix} = \begin{pmatrix} M_{11} & M_{12} \\ M_{21} & M_{22} \end{pmatrix} \begin{pmatrix} E_L^+ \\ E_L^- = 0 \end{pmatrix}, \quad (7)$$

which differs from the physical Fresnel case, Eq. (2), because there is no incoming source term ( $E_1^+ = 0$ ). It is possible to re-express Eq. 11 into the form of a homogeneous equation that maps

the outgoing ( $E_1^-$ ,  $E_L^+$ ) waves defined in relation to the central structure onto the (zero-valued) incoming or source waves ( $E_1^+$ ,  $E_L^-$ ) and so the modes are often referred to as being solutions of a homogeneous equation. It is easy to see that Eq. 11 is satisfied if  $M_{1,1} = 0$ . In general this condition cannot be satisfied with the real value of  $k_x$  used to solve the physical Fresnel equations as in Sec. IIA above. Rather, one must extend  $k_x$  into the complex plane,

$$k_x = \beta + i\alpha, \quad (8)$$

and see if one or more complex values of  $k_x$  can be found such that  $M_{1,1} = 0$ . Furthermore, it is then the case that all the  $k_{zi}$  are complex, which means that there can be a variety of exponentially decaying and growing possibilities for regions 1 and  $L$  depending on the sign of  $k_{zi}$ . Several of these solutions may correspond to physically relevant modes. There are several important symmetries to be aware of. First, as already noted in the case of the physical Fresnel equations, the solutions are unchanged by sign permutation of  $k_z$  in the absorbing layers [1]. Second, regarding the outer layers, it is the case that if  $M_{1,1}(k_{z1}) = 0$ , then  $M_{2,1}(-k_{z1}) = 0$  and similarly for  $k_{zL}$ . Since the reflection is proportionate to  $M_{2,1}$  (see Eqs. (3) and (5)) this means that the existence of a mode (i.e.,  $M_{1,1} = 0$ ) with one choice of sign for  $k_{z1}$  leads to a reflection zero with the opposite sign choice.

Some authors have considered designating the modes by the sign of  $\text{Im}(k_{zi})$  in the dielectric layers [3]. One particularly appealing choice of signs of the imaginary parts that is often invoked is one that leads to exponential decay away into the  $j = 1$  and  $j = L$  layers, which represents a purely bound mode. However, we have found (Sec. III) that such requirements on just the imaginary parts do not necessarily lead to modal dispersions that are continuous in frequency. Alternatively, we suggest minimal constraints on the waveforms in the dielectric layers that lead to distinct, continuous dispersions for the modes supported by the  $L$ -layer structure. We choose these constraints in correspondence to physically intuitive scenarios, focusing on the exponential behavior of the mode into the superstrate layer of the structure and the direction of travel of the mode on the substrate side. This allows straightforward connection to the K-R experiment. We focus on two such scenarios that have particular relevance to K-R experiments: Case (1), when the mode is evanescent into layer  $L$  and incoming in layer 1, and Case (2), when the mode is evanescent into layer  $L$  and outgoing in layer 1 (see Fig. 2). This corresponds to solving

$$\begin{aligned} M_{1,1}(\beta, \alpha) &= 0 \\ \text{s.t. } \text{Im}(k_{zL}) &> 0 \text{ and } \text{Re}(k_{z1}) < 0 \end{aligned}$$

for Case (1) and

$$\begin{aligned} M_{1,1}(\beta, \alpha) &= 0 \\ \text{s.t. } \text{Im}(k_{zL}) &> 0 \text{ and } \text{Re}(k_{z1}) > 0 \end{aligned}$$

for Case (2). We further classify a scenario that is reciprocal to Case (2) as Case (3) (see Fig. 2), which corresponds to solving

$$\begin{aligned} M_{1,1}(\beta, \alpha) &= 0 \\ \text{s.t. } \text{Im}(k_{z1}) &> 0 \text{ and } \text{Re}(k_{zL}) > 0. \end{aligned}$$

However, Case (3) is not generally compatible with K-R experiments because of the evanescent structure into the glass. As such, we will not focus in detail on the Case (3) modes in this paper.

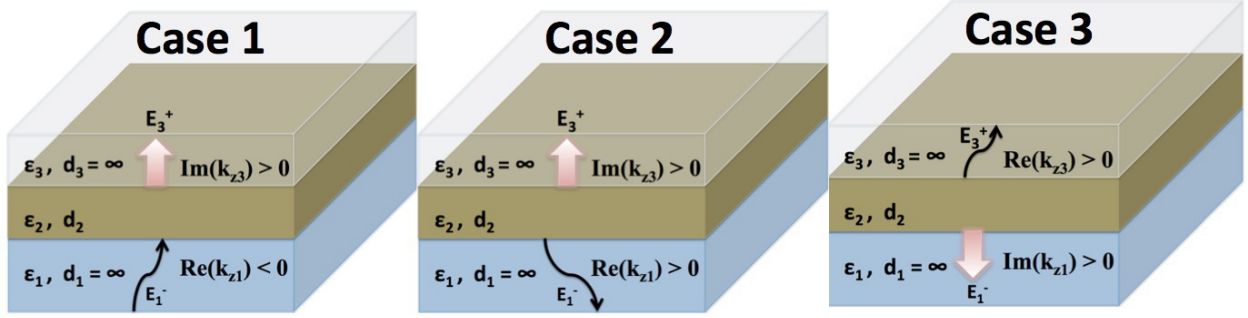


Figure S2: Schematic of conditions on wavevectors in dielectric layers that the Case (1), Case (2), and Case (3) modes. Case 1, which is evanescent into dielectric layer 3 and has incoming waves in the substrate, gives rise to the perfectly absorbing mode. Case 2, which is evanescent into the dielectric layer 3 and has outgoing waves in the substrate, gives rise to the SPP supported on the surface between layer 2 and 3. Case 3, which is evanescent into the dielectric layer 1 and has outgoing waves in the superstrate layer 3, gives rise to a mode which has evanescent structure at the interface between the substrate and the absorbing layer.

In practice these solutions are obtained by minimizing  $|M_{1,1}(\beta, \alpha)|$  while choosing the signs of  $k_{z1}$  and  $k_{zL}$  to be such that the inequalities above are true and, of course, verifying that the solution(s) so obtained are actually zeros of  $M_{1,1}$ . Because of the non-zero character of both outgoing and incoming components in the interior layers, the results do not depend on the choice of their  $k_z$  components. We employ the simplex method [4] for this purpose and for each  $\omega$  a large number of random initial guesses in  $\beta, \alpha$  are tried with the simplex procedure applied to each one. In such a fashion it is possible that one or more unique solutions might be found for each  $\omega$ .

## Connection of Case 1 Mode to Equations for PA Mode

In the main text, we present equations for the PA mode that are consistent with incoming wave conditions, or driving by an external field. Here we comment on the connection to this formulation, and the formulation above with the homogeneous equations with the Case 1 conditions on the wavevector components.

The PA mode may be defined by satisfying the following:

$$M_{1,1}(\beta, \alpha) = 0$$

s.t.  $\text{Im}(k_{zL}) > 0$  and  $\text{Re}(k_{z1}) < 0$

This has implications for the electric field in layer 1, namely that it is proportional to

$$E_1^- \exp(i|k'_{z1}|z) \exp(-k''_{z1}) \quad (9)$$

which is clearly an incoming wave!

Here it is important to note the following symmetry relation: if  $M_{1,1}(k_{z1}) = 0$ , then  $M_{2,1}(-k_{z1}) = 0$  and similarly for  $k_{zL}$ . However, we cannot say in general that if  $M_{1,1}(k_{z1}) = 0$ , then  $M_{1,1}(-k_{z1}) \neq 0$ .

Recall we define the reflection amplitude as the outgoing wave amplitude in layer 1 divided by the incoming wave amplitude in layer 1. This can be written as

$$r = \frac{E_1^-}{E_1^+} = \frac{M_{2,1}}{M_{1,1}} \quad (10)$$

provided  $E_1^-$  is outgoing and  $E_1^+$  is incoming. This will only be the case when  $\text{Re}(k_{z1}) > 0$ . Hence, if we want to compute the reflection amplitude at the position of Mode 1, we must multiply  $k_{z1}$  by -1 to obtain the proper sign convention for computing it. At this point, we can invoke the symmetry relation written above to see that  $M_{2,1} = 0$ , meaning that the reflection amplitude is zero for mode 1! That is, we see that the outgoing wave amplitude is zero and there is non-zero incoming wave amplitude.

A completely equivalent way to find this mode is to write the equations with finite incoming wave amplitude and 0 outgoing wave amplitude along with choosing conventions for  $\text{Re}(k_{z1}) > 0$  so that  $E_1^-$  is outgoing and  $E_1^+$  is incoming. One writes this as

$$\begin{pmatrix} E_1^+ \\ E_1^- = 0 \end{pmatrix} = \begin{pmatrix} M_{11} & M_{12} \\ M_{21} & M_{22} \end{pmatrix} \begin{pmatrix} E_L^+ \\ E_L^- = 0 \end{pmatrix}, \quad (11)$$

where an equivalent solution to mode 1 is found when

$$\begin{aligned} M_{2,1}(\beta, \alpha) &= 0 \\ \text{s.t. } \text{Im}(k_{zL}) &> 0 \text{ and } \text{Re}(k_{z1}) > 0. \end{aligned}$$

Hence, we see that formulation we proposed in the main text for the PA dispersion that contained a driving field in region 1 as a boundary condition is completely equivalent to the solving the homogeneous equation under the constraint that the  $\text{Re}(k_{z1}) < 0$  and  $\text{Im}(k_{zL}) > 0$ . In either case, the solution is a mode that exists in the presence of an incoming (driving) field from region 1 and corresponds to perfect extinction of the incoming field. The mode is in fact a zero in the reflectance in the complex plane, and this zero influences the magnitude of reflected light measured in the far-field or computed by the Fresnel equations along the real axis. It is the presence of this mode, not the SPP mode, that gives rise to the minimum in reflectance measured in K-R experiments.

## Results from 3-Layer structure

Consistent conclusions can be drawn from results involving a single thin metal film in the K-R geometry, for example, a glass/gold/air structure. Fig. S3 shows results from a simulated K-R experiment with 532 nm light resonant with the SPP mode (at  $45.8^\circ$ ) in panel **a**) and resonant with the PA mode (at  $48^\circ$ ) in panel **b**). Consistent with the glass/germanium/gold/air structure presented in the main text, we see that the PA mode only exists in the driven region, and that the freely-propagating mode corresponds to the SPP mode. In Fig. S4, we again see that the transmission amplitude maximum corresponds to the angle resonant with the SPP mode and the reflectance minimum corresponds to the angle resonant with the PA mode. We note also that the germanium underlayer exaggerates the disparity between the PA and SPP modes at higher frequencies where the losses are larger (see Fig. S5).

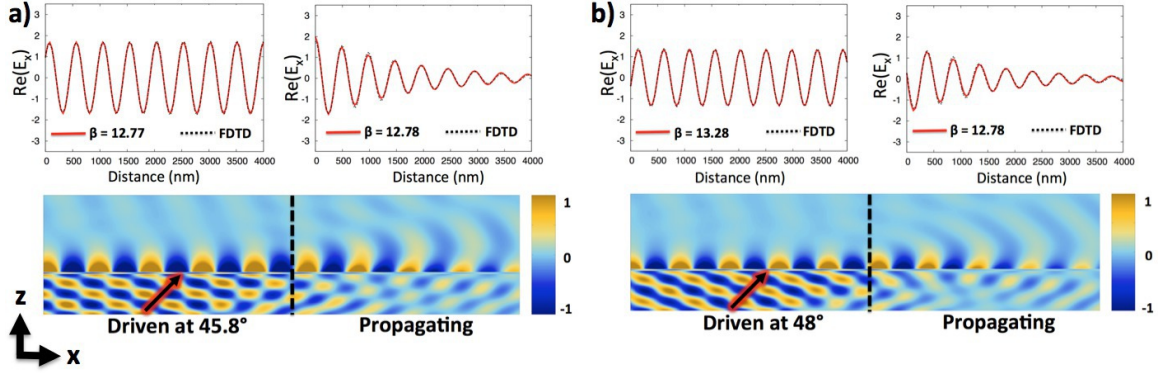


Figure S3: FDTD simulation of K-R excitation of SPPs on glass/50 nm Au/air structure. The “Driven Region” and is directly illuminated with 532 nm light, whereas in the “Propagating” region, the SPP propagates freely without illumination. The real  $x$ -component of the phasor field is sampled 50 nm above the gold surface and fit to the functional form  $A\cos(\beta x - \omega t_0)$  in the Driven region and  $A\cos(\beta x - \omega t_0) \exp(\alpha x)$  in the propagating region. In K-R excitation at  $45.8^\circ$ , resonant with the SPP mode **a)** and at  $58^\circ$ , resonant with the PA mode **b)**, the propagating SPP (in the Propagating region) has a value of  $\beta$  in good agreement with the SPP dispersion,  $\beta = 12.77\mu\text{m}^{-1}$ .

## Comparison of Modal Solutions to Semi-Infinite SPP dispersions

The dispersions of the SPP and PA modes for the glass/50 nm Au/air structures are plotted in Fig. S5a in comparison with the semi-infinite gold/air SPP dispersion. This shows the clear close agreement between the SPP mode and the semi-infinite gold/air SPP dispersion. Similarly, the SPP and PA modes for the glass/50 nm Au/air structures are plotted in Fig. S5b, also in comparison with the semi-infinite gold/air dispersion. This shows that the germanium underlayer strongly perturbs the PA mode in the higher frequency regions, but leaves the SPP mode relatively unchanged.

## Finite-Difference Time-Domain Simulations

A commercial-grade simulator based on the finite-difference time-domain (FDTD) method was used to perform these numerical K-R experiments (<http://www.lumerical.com/tcad-products/fdtd/>) for simulating the K-R and leakage experiments. The permittivity of gold is fit to data by Johnson and Christy [5], permittivity of germanium is fit to data by Palik [6], and a static value of 1.51 and 1.0 is used for glass and air, respectively. To simulate the K-R experiment, a 2-D computational domain (6 microns in  $x$ , 1 micron in  $z$ ) with grid size of 1 nm in  $x$  and  $z$ . A plane-wave source is used in the driven region. A similar setup is used to simulate the leakage experiment (3 microns in  $x$ , 1.2 microns in  $z$ ). A plane wave source spanning the 3 micron region is placed above the gold film that illuminates two  $r=100$  nm gold spheres on the surface. A series of simulations are performed with spacing between the NPs ranging including 0.8, 1.0, 1.2, 1.4, and 1.6 microns. Radiation in the far field in the substrate side is collected to quantify the leakage radiation. An average is taken of the

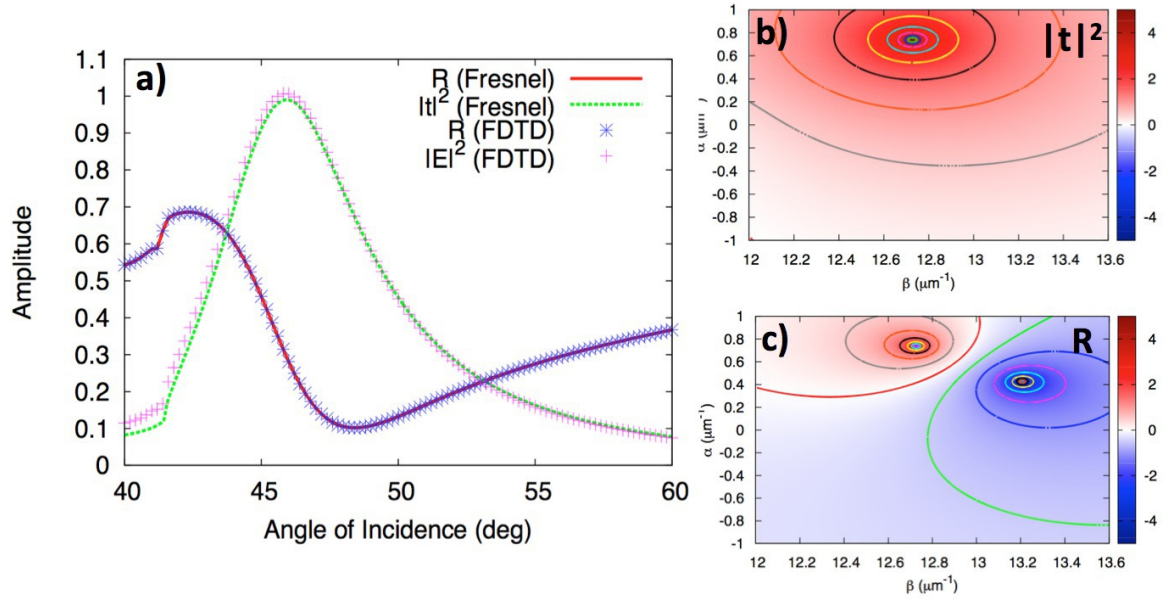


Figure S4: Light incident from glass substrate for structures illustrated in Fig. 2 with nearly-resonant incident angles excites an evanescent field on the gold/air surface. The Fresnel reflection ( $R$ ) and the squared magnitude of the transmission amplitude ( $|t|^2$ ) for light incident from glass side are plotted in (a). For comparison, the electric field intensity ( $|\mathbf{E}|^2$ ) of the evanescent field 10 nm above the gold surface is computed by the FDTD method and plotted, showing that it very closely follows  $|t|^2$ . FDTD is also used to numerically calculate the reflection of the structure, which is shown to be in excellent agreement with the Fresnel calculation. Note that both  $|\mathbf{E}|^2$  and  $|t|^2$  are normalized to their respective maximum values across the range of angles considered. The  $|t|^2$  and  $R$  surface in the complex  $\beta - \alpha$  plane at 532 nm for the glass/50 nm Au/air structure is plotted in b), showing that the SPP mode corresponds to an infinity in  $|t|^2$  and  $R$ , while the PA mode corresponds to a zero in  $R$ .

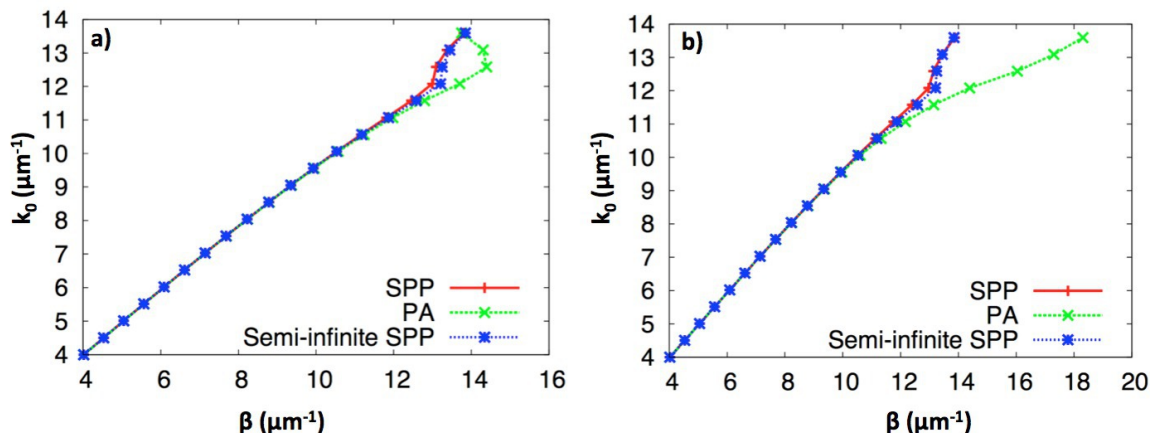


Figure S5: **a)** Comparison of PA and SPP modes for 50 nm gold between glass and air to semi-infinite SPP dispersion. **b)** Comparison of PA and SPP modes for 4 nm Ge/ 50 nm gold between glass and air to semi-infinite SPP dispersion.

leakage radiation from all of these calculations to simulate the ensemble average over various NP spacings in the real experiment.

### Scaling of Experimental and Fresnel Data in Fig. 3

While the Fresnel reflectance will always fall between 0 and 1, the square of the Fresnel transmission amplitude and the evanescent wave nearfield enhancement may exceed 1. Only the relative magnitudes are important to our arguments, particularly the positions of the maxima and minima, so we scale  $|t|^2$  and  $|E|^2$  by an arbitrary factor so that the relative magnitudes are comparable to the Fresnel reflectance for ease of interpretation of the figures.

The intensity scale of the experimental reflectance and leakage, as well as the averaged FDTD leakage, are also arbitrary. Furthermore, an absolute reference point indicating  $0^\circ$  in our experiments cannot be identified, which leads to a potential systematic error of between  $-1$  and  $1^\circ$  in the reflectance and leakage. We determine the magnitude of this systematic error by aligning the experimental reflectance spectrum with the Fresnel reflectance, as the two should be identical provided the geometry and material properties of the films are known. We determine that the measured reflectance angle must be shifted by  $+1^\circ$ , and we apply this shift to the leakage measurements, as well. Finally, the experimental and simulated leakage intensities are scaled so that the local maximum near the SPP leakage angle has an amplitude of 1. From the standard deviation of the leakage and reflectance data samples over various cuts through the 2-D images, we estimate the signal to noise ratio to be approximately 5.

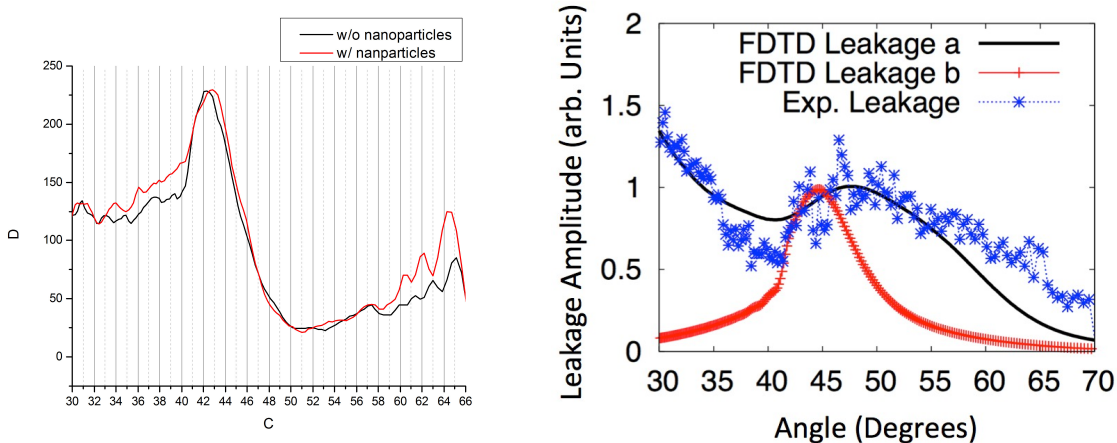


Figure S6: (Left) Comparison of reflectance with and without nanoparticles, demonstrating that NPs have negligible effect on position of the PA resonance at the frequency of interest. (Right) Comparison of experimental leakage with FDTD simulation of leakage in R-K configuration with nanoparticles on the gold surface (FDTD Leakage a), as well as FDTD simulation of leakage in R-K configuration on a bare gold surface (no nanoparticles, FDTD Leakage b). The nanoparticles serve mostly to broaden the leakage signal. While the leakage maximum is shifted by +3 degrees by the nanoparticles ( $47.5^\circ$  compared to  $44.7^\circ$ ), the maximum is still distinct from the reflectance minimum at  $54^\circ$ . The simulations for FDTD Leakage b used a dipole source to couple into SPP modes.

## Effect of nanoparticles on Reflectance Spectrum

We measured the reflectance of the gold/germanium substrate with and without the nanoparticles to confirm that the presence of nanoparticles does not significantly affect the position of the PA resonance.

## Further distinction between SPP and PA modes

In the examples presented in the main text, both PA and SPP modes can be found. Indeed, the mode we identify as the PA mode has certain commonalities with the SPP mode, as can be seen with the charge-density oscillations evident in the fields in Fig. 4. However, we maintain that the PA phenomena can be observed in cases when SPPs cannot. We consider examples of PA modes reported by Capasso and co-workers in Ref. [7,8], which involve a structure of optically thick sapphire with a 180 nm layer of VO<sub>2</sub> with air above, and optically thick gold, coated with a 4 nm layer of germanium with air above, respectively. Both can be analyzed in a similar fashion as the modes we present in our work. Here, one finds a zero in the reflectance in the complex plane of wavevector components (beta and alpha, in our notation), which is how we define the PA mode. The positions of this mode is associated with reflectance minima as measured experimentally or computed via the Fresnel equations. We rule out SPPs as influencing the reflectance minima for two reasons for these

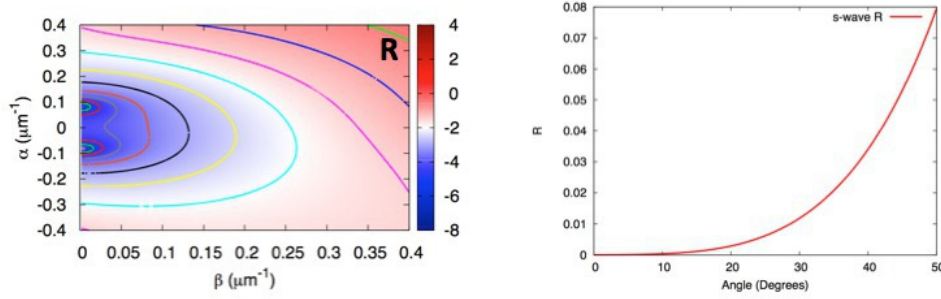


Figure S7: Plot of s-polarized reflectance and transmission amplitude surfaces, along with Fresnel reflectance for optically thick Saphire coated with 180 nm  $\text{VO}_2$  illuminated 11.75 micron light from air above. The near perfect absorbance in this structure is due to the presence of the PA mode, as defined by the zero in  $R$  as a function of  $\beta$  and  $\alpha$ , and is not due to the presence of an SPP mode, which is prohibited for two reasons: the excitation source is within the air light cone, and the excitation source is s-polarized. Note the Fresnel reflectance minimum occurs at  $\theta = 0^\circ$ , or  $\beta = 0.0\mu\text{m}^{-1}$ . The mapping between  $\beta$  and  $\theta$  is given by  $\theta = \sin^{-1}(\frac{\beta}{k_0})$  where  $k_0 = 0.55\mu\text{m}^{-1}$ .

particular instances: (1) The reflectance minima are found when illuminating from the air side, meaning they are inside the air light cone, and (2) the reflectance minima (and the PA modes) can be found with both p- and s-polarized excitation sources. Both (1) and (2) are incompatible with SPPs which, by definition, exist outside of the air light cone, and cannot be excited by s-polarized light. Representative figures for the s- and p-wave modes in Ref. [7] are given in Fig. S7 and S8.

1. Yeh, P. *Optical waves in layered media* (Wiley, 2005).
2. Montgomery, J. M.; Gray, S. K. Enhancing surface plasmon polariton propagation lengths via coupling to asymmetric waveguide structures. *Phys. Rev. B* **2008**, *77* 125407-125415.
3. Brissinger, D; Salamon, L.; De Fornel, F. Unguided plasmon-mode resonance in optically excited thin film: exact modal description of Kretschmann-Raether experiment. *J. Opt. Soc. Am. B* **2013**, *30* 333-337.
4. Nelder, J. A.; Mead, R. A simplex method for function minimization. *Comp. J.* **1965**, *7* 308-313.
5. Johnson, P. B.; Christy, R. W. Optical constants of the noble metals. *Phys. Rev. B* **1972**, *6* 4370-4379.
6. Palik, E. D. *Handbook of optical constants of solids* (Academic Press, 1998).
7. M. A. Kats, D. Sharma, J. Lin, P. Genevet, R. Blanchard, Z. Yang, M. M. Qazilbash, D. N. Basov, S. Ramanathan, and F. Capasso, *App. Phys. Lett.* **2012**, *101* 221101-221106
8. M. A. Kats, R. Blachard, P. Genevet, and F. Capasso, *Nat. Mat.* **2013**, *12* 20-24

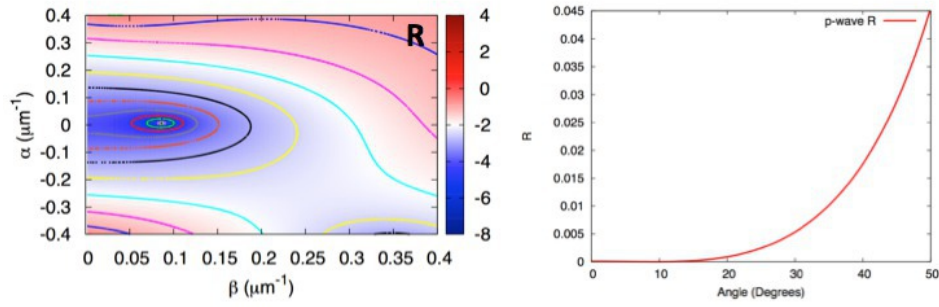


Figure S8: Plot of p-polarized reflectance and transmission amplitude surfaces, along with Fresnel reflectance for optically thick Sapphire coated with 180 nm  $\text{VO}_2$  illuminated 11.75 micron light from air above. The near perfect absorbance in this structure is due to the presence of the PA mode, as defined by the zero in  $R$  as a function of  $\beta$  and  $\alpha$ , and is not due to the presence of an SPP mode, which is prohibited because the excitation source is within the air light cone. Note the Fresnel reflectance minimum occurs at  $\theta = 9^\circ$ , or  $\beta = 0.08\mu\text{m}^{-1}$ . The mapping between  $\beta$  and  $\theta$  is given by  $\theta = \sin^{-1}(\frac{\beta}{k_0})$  where  $k_0 = 0.55\mu\text{m}^{-1}$ .